Old Dominion University
ODU Digital Commons

CCPO Publications | Center for Coastal Physical Oceanography

2006

Topographic Influence on Overflow Dynamics: Idealized Numerical Simulations and the Faroe Bank Channel Overflow

Tal Ezer
Old Dominion University, tezer@odu.edu

Follow this and additional works at: https://digitalcommons.odu.edu/ccpo_pubs

 Part of the Oceanography Commons

Repository Citation

Ezer, Tal, "Topographic Influence on Overflow Dynamics: Idealized Numerical Simulations and the Faroe Bank Channel Overflow" (2006). *CCPO Publications*. 127.
https://digitalcommons.odu.edu/ccpo_pubs/127

Original Publication Citation

Ezer, T. (2006). Topographic influence on overflow dynamics: Idealized numerical simulations and the Faroe Bank Channel overflow. *Journal of Geophysical Research: Oceans, 111*(2). doi: 10.1029/2005JC003195

This Article is brought to you for free and open access by the Center for Coastal Physical Oceanography at ODU Digital Commons. It has been accepted for inclusion in CCPO Publications by an authorized administrator of ODU Digital Commons. For more information, please contact digitalcommons@odu.edu.

Topographic influence on overflow dynamics: Idealized numerical simulations and the Faroe Bank Channel overflow

Tal Ezer

Program in Atmospheric and Oceanic Sciences, Princeton University, Princeton, New Jersey, USA

Received 1 August 2005; revised 6 October 2005; accepted 9 November 2005; published 10 February 2006.

[1] Properties of the North Atlantic Deep Water (NADW) depend on mixing that occurs in the Denmark Strait (DS) and the Faroe Bank Channel (FBC) overflow regions. How the sill's topography in those regions may affect mixing processes and downstream variability is thus investigated using a high-resolution terrain-following ocean model. Model results agree with observations that show enhanced mixing and entrainment downstream from the sill; however, mixing seems to occur over a longer distance downstream from the FBC sill and more abruptly downstream from the DS sill. Sensitivity experiments with various FBC sill widths demonstrate that the narrow sill is responsible for the enhanced mixing. The downstream flow variability, eddy propagation, and deep water properties are affected by sill width and background stratification. Similar to the laboratory overflow experiments of Cenedese et al. (2004), three distinct mixing regimes (characterized by the Froude number) are identified in the FBC simulations: a steady subcritical flow regime upstream from the sill, a supercritical wave-like flow regime downstream from the sill, and an irregular eddy-dominated regime farther away from the sill. Satellite altimeter data near the FBC show cyclonic anomalies propagating along the northern slope of the channel, resembling the surface eddies associated with the overflow variability in the model. A cross-channel circulation over the FBC sill, driven by frictional bottom boundary layers, resulted in convergence/divergence zones near the southern/northern slopes and pinching/spreading of isotherms across the channel, similar to the observation-based mechanism proposed by Johnson and Sanford (1992).

Citation: Ezer, T. (2006), Topographic influence on overflow dynamics: Idealized numerical simulations and the Faroe Bank Channel overflow, *J. Geophys. Res.*, *111*, C02002, doi:10.1029/2005JC003195.

1. Introduction

[2] The North Atlantic Deep Water (NADW) mass provides one of the most important sources for the deep water of the world oceans. The NADW originates from the Greenland Sea, but must pass through relatively shallow sills where dense overflow waters mix with overlying layers. Thus the NADW properties largely depend on transports, mixing and entrainment that occur in two overflow regions: the Denmark Strait Overflow (DSO) region and the Faroe Bank Channel Overflow (FBCO) region (Figure 1). Possible global climate changes may be connected to transport changes in the overflow regions [*Hansen et al.*, 2001]. The two overflow regions are quite different in their topography and water properties. The DSO region includes a wide (~100 km) and shallow (~600 m) sill where waters spill into the continental slope and produce strong entrainment and eddy activities downstream of the sill [*Bruce*, 1995; *Krauss*, 1996; *Krauss and Käse*, 1998; *Jungclaus et al.*, 2001; *Käse et al.*, 2003; *Girton and Sanford*, 2003]. The FBC on the other hand is a narrow sill (~20 km wide) which connects to the relatively wide Faroe-Shetland Channel upstream and to the continental slopes of the Iceland Basin downstream. Figure 2 (using results presented by *Mauritzen et al.* [2005]) shows typical observed sections across and along the channel, demonstrating the remarkable changes in structure that the overflow waters undergo on their way across the sill. At over 800 m sill depth, the FBC provides the deepest connection between the Nordic Seas and the North Atlantic. Various observational studies of the FBC region were conducted over the years [*Borenäs and Lundberg*, 1988, 2004; *Saunders*, 1990; *Johnson and Sanford*, 1992; *Price and Barringer*, 1994; *Høyer and Quadfasel*, 2001; *Borenäs et al.*, 2001; *Saunders*, 2001; *Duncan et al.*, 2003; *Geyer et al.*, 2005; *Lake et al.*, 2005; *Mauritzen et al.*, 2005]. Some of the interesting findings of these studies include enhanced mixing, bottom drag and eddy variability downstream from the sill, oscillatory flows with periodicity of 3–6 days and an asymmetric isotherm structure across the sill (Figure 2, section D), with pinched isotherms on the Faroe Bank (southern) side and spread out isotherms on the Faroe Islands (northern) side. Different mechanisms have been proposed to explain the observed structure and variability near the sill, but the

Copyright 2006 by the American Geophysical Union.
0148-0227/06/2005JC003195

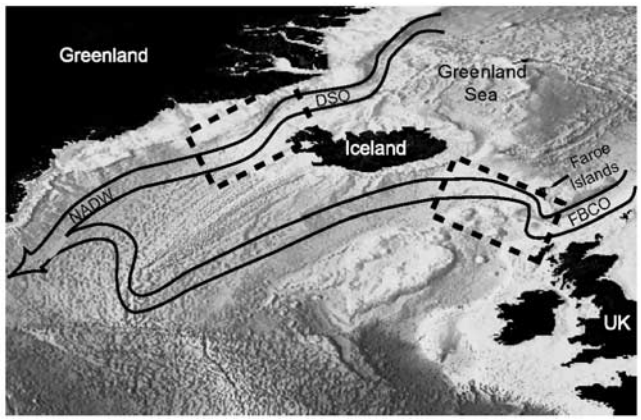

Figure 1. Seafloor bottom topography (data based on work by *Smith and Sandwell* [1997]) and schematic of the two main routes of the overflow waters that form the North Atlantic Deep Water (NADW): the Denmark Strait Overflow (DSO) and the Faroe Bank Channel Overflow (FBCO). The dashed boxes represent the regions of interest simulated in this study.

dynamics is still not completely understood [for more details, see for example the review papers by *Hansen and Østerhus*, 2000; *Saunders*, 2001; *Borenäs and Lundberg*, 2004]. Some of these observed phenomena (which are also evident in the model results as shown later) motivated this study which aims to investigate the role of the sill topography in the mixing and downstream dynamics of overflows.

[3] Unlike the many (realistic and idealized) high-resolution modeling studies of the DS region [e.g., *Jiang and Garwood*, 1996; *Käse et al.*, 2003; *Jungclaus et al.*, 2001; *Ezer*, 2005; *Legg et al.*, 2006], only a few high-resolution numerical model studies of the Faroese Channels region have been conducted in the past [e.g., *Oey*, 1998], though now there are renewed modeling efforts in the area [e.g., *Riemenschneider and Legg*, 2005]. The regional models provide better understanding of the overflow dynamics and may help in parameterization of mixing in large-scale models. Coarse resolution global climate models do not usually resolve the overflow regions and may require some bottom boundary layers or entrainment parameterizations [*Price and Barringer*, 1994; *Adcroft et al.*, 1997; *Beckmann and Döscher*, 1997; *Winton et al.*, 1998; *Pacanowski and Gnanadesikan*, 1998; *Campin and Goosse*, 1999; *Killworth*

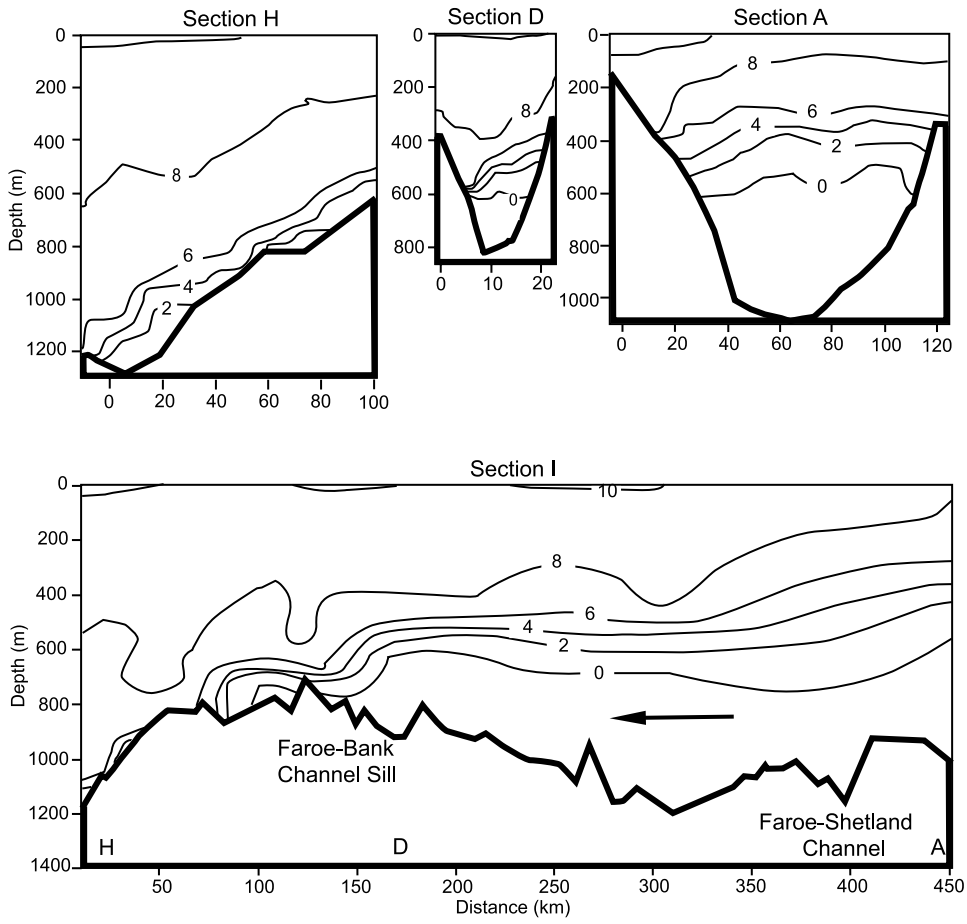

Figure 2. Examples of observed potential temperatures (in degrees Celsius) from the Faroese Channels (using results presented by *Mauritzen et al.* [2005]): (top) sections across the Faroe-Shetland Channel upstream of the sill (section A), across the Faroe-Bank Channel near the sill (section D), and across the continental slope downstream from the sill (section H) and (bottom) section I taken along the channels. The general flow direction and the location of the across-channel sections are marked.

and Edwards, 1999; *Song and Chao*, 2000; *Hallberg*, 2000]. Various idealized numerical models can provide important tools to study overflow processes [*Jiang and Garwood*, 1996; *Jungclaus and Mellor*, 2000; *Käse et al.*, 2003; *Jungclaus et al.*, 2001; *Ozgokmen and Chassignet*, 2002; *Papadakis et al.*, 2002; *Ezer and Mellor*, 2004; *Ezer*, 2005; *Legg et al.*, 2006]. For example, the Dynamics of Overflows Mixing and Entrainment (DOME) initiative established an idealized model setup, resembling the conditions of the DSO, to investigate the dynamics of bottom plumes and a standard framework to compare different models. The DOME setup was used to compare terrain-following and *z* level models [*Ezer and Mellor*, 2004; *Ezer*, 2005], and to compare isopycnal and *z* level models as well as hydrostatic and nonhydrostatic models [*Legg et al.*, 2006]. At high enough resolutions and good mixing schemes idealized models can simulate quite well some of the observed overflow properties despite some simplified and unrealistic features of the DOME configuration relative to the real topography of the DS. *Ezer* [2005] shows that when using the Mellor-Yamada (M-Y) turbulence scheme [*Mellor and Yamada*, 1982] in a terrain-following ocean model with 2.5 and 10 km resolutions, one can produce bottom plume dilution and eddy structure strikingly similar to that obtained by a 0.5 km nonhydrostatic model. However, the results also indicate a complex, spatially varying mixing coefficient (resulted from the prognostic equations of the M-Y scheme) that may vary by over two orders of magnitude across the bottom plume. It is thus quite difficult to reproduce such a structure with simple mixing parameterizations and coarser resolution models. A similar spatial mixing coefficient structure has been observed and modeled in bottom boundary layers found in other regions [e.g., *Ezer and Weatherly*, 1990]. It is interesting to note that enhanced mixing downstream from the FBC has been suggested on the basis of observations, but the estimated turbulent diffusivities range from $\sim$100 to $\sim$1000 $\times$ 10^{-4} m^2 s^{-1} [*Saunders*, 1990; *Duncan et al.*, 2003; *Mauritzen et al.*, 2005]; these values may be 3–4 orders of magnitude larger than the mixing in the abyssal ocean away from bathymetric features. *Mauritzen et al.* [2005] also noted that strong overflow mixing extends for a relatively long distance downstream from the FBC compared with a more abrupt mixing near the DS.

[4] This study is a followup of *Ezer and Mellor* [2004], *Ezer* [2005], and *Legg et al.* [2006], that used the DOME configuration, but here additional experiments using new idealized configurations that resemble the FBC region are added. These experiments will help us to evaluate the sensitivity of the overflow mixing and dynamics in the model to the topography of the sill region, and to some extent to interpret some observed features. The paper is organized as follows. First in section 2 the model setup and configurations are described, then in section 3 model results are analyzed and compared with some observations. Finally, discussion and conclusions are offered.

2. Ocean Model Setup and the Sensitivity Experiments

[5] The generalized coordinate ocean model, described in detail by *Mellor et al.* [2002], was derived from the free surface, three-dimensional, primitive equation Princeton Ocean Model (POM) of *Blumberg and Mellor* [1987]. However, the standard terrain-following (sigma) coordinates are replaced with a more general vertical grid that can include any combination of terrain-following or *z* level distributions or even an adaptive grid that may vary in space and time. Here only results using terrain-following vertical grids are presented for consistency in the comparison with previous terrain-following calculations. Exploration of the sensitivity of overflow simulations to different types of vertical coordinates and various horizontal resolutions can be found in work by *Ezer and Mellor* [2004], *Ezer* [2005], and *Legg et al.* [2006].

[6] Several different idealized configurations with a 1000 $\times$ 500 km domain, 25 sigma layers (with higher resolution near the bottom) and 2.5 km horizontal grid size are used here; see Figure 3 for details. The first model configuration is the so-called DOME setup, described by *Ezer and Mellor* [2004], *Ezer* [2005], and *Legg et al.* [2006]. In this case, a flat bottom embayment, 100 km wide and 600 m deep, represents the Denmark Strait, where dense source waters are injected and spilled directly into a 1% steep slope. Though this configuration is clearly an extreme simplification of the real DS topography it provides the simplest benchmark for idealized model comparisons, and surprisingly, produces some of the observed mixing and bottom plume properties. The second configuration, named FBC (Faroe Bank Channel, Figure 3b), has a 500 km long channel (narrowest at the sill, where water depth is 800 m, and widest where it connects to the slope). The channel cross section is parabolic, which seems to be a good estimate of the real topography [*Borenäs and Lundberg*, 1988; *Lake et al.*, 2005]. Four different variations of the FBC configuration are used. The intermediate sill width case shown in Figure 3b is named FBC-40 experiment (sill width = 40 km). Another experiment with the same topography is FBC-40-NS (no background stratification). Two other experiments with narrow (FBC-20 km) and wide (FBC-80 km) sills are used to test the sensitivity of the results to the sill's width. Except the NS case, the initial background stratification in the domain includes a linear density distribution as a function of *z*; the density of the source water is the same as that of the deepest regions. (Thus, if there were no entrainment or mixing, one would expect the source water to reach the bottom of the deepest ocean after a long time; this of course, is not the case in either in the model or in the real ocean.) A linear equation of state (with a constant salinity value) is used. Since the density in the FBC is uniquely determined by the temperature [*Borenäs and Lundberg*, 2004], this assumption may not be so unreasonable. The initial maximum density difference between the surface and the deepest layers, and between the surface and the dense source waters are 2 kg m^{-3} for the DOME case and 1 kg m^{-3} for the FBC case. These values are somewhat larger than observed values (especially for the DOME case, but this is the value used by the previous model intercomparison studies so it is left unchanged). However, one has to keep in mind that the idealized experiments are an initial value problem, assuming that initially there is no trace of the source waters in the interior and that the source must be as dense as the deepest ocean, while observations represent upstream and down-

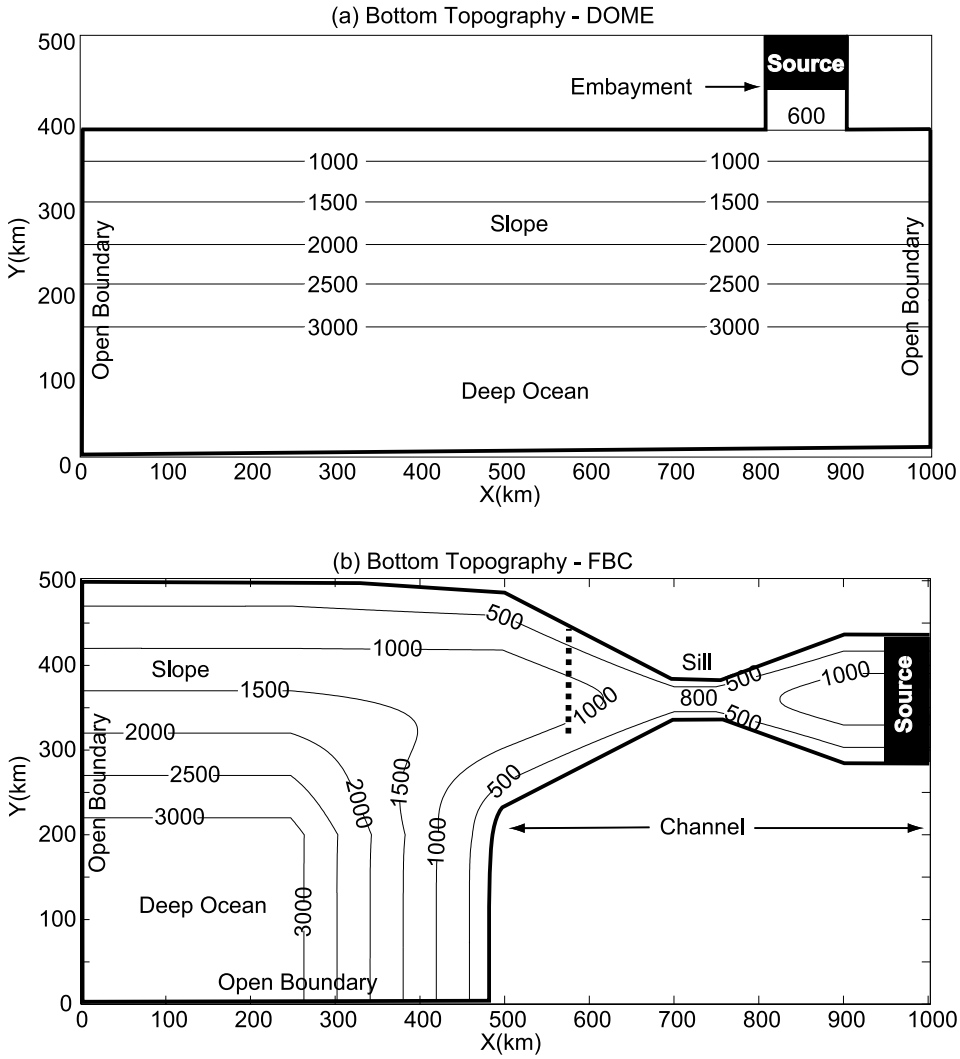

Figure 3. Idealized topography of the model domains: (a) DOME configuration and (b) FBC configuration. Depth contours are in meters. Dark regions indicate the buffer zones where the dense source waters are imposed. The dashed vertical line in Figure 3b indicates the location of the section shown in Figure 5. The bathymetry in Figure 3b is for the intermediate sill width cases (experiments FBC-40 and FBC-40-NS); the bathymetry for the narrow sill width (experiment FBC-20) and for the wide sill width (experiment FBC-80) are similar except in the sill area (700 km < x < 750 km).

stream water properties that already have been mixed over a long period of time. Taking into account some (unavoidable) mixing in the vicinity of the imposed source, the dense waters reached the sill with properties more similar to the observation than those at the source itself. For the FBC case the observed density difference between the North Atlantic Water mass and the FBC bottom waters of 0.5 to 0.8 kg m^3 [*Price and Barringer*, 1994; *Mauritzen et al.*, 2005] is not too far from the model density, where the temperature difference of ~8°C a few kilometers from the imposed source is quite similar to the observed profiles in the Faroe-Shetland Channel (Figure 2, section A). In the DOME case the imposed near-bottom dense source is in a geostrophic balance with maximum thickness of 300 m near the west wall of the embayment and exponentially thinning to zero near the eastern wall (to minimize mixing in the embayment itself); the source transport is maintained at 5 Sv (1 Sverdrup = 10^6 m^3 s^{-1}), somewhat larger than the estimated transport of ~3 Sv. In the FBC case, the imposed source waters are 800 m thick across the channel (near the eastern wall, Figure 3b). The velocities are not imposed, allowing them to dynamically adjust to the baroclinic structure and topography, including the formation of a return upper ocean flow above the overflow. The result is an overflow transport at the sill of 2.5 Sv for the FBC-20 case, 3.2 Sv for the FBC-40 case and 3.7 Sv for the FBC-80 case. Estimated bottom transports from observations (i.e., for ~20 km sill width) are generally ~2 Sv, but there are time-dependent variations in the range 1–3.5 Sv [*Mauritzen et al.*, 2005]. To help analyze the development of the dense water plume, a tracer, with value $c = 1$, was injected into the dense water source; initially $c = 0$ everywhere else. In a later time after mixing occurs the bottom plume interface is defined by $c = 0.01$. While the setup configuration is very idealistic and aimed mainly for sensitivity model studies, it nevertheless reproduces some of the observed properties of

the overflow quite well, as shown before for the DOME case and as will be shown here for the FBC case.

3. Results

3.1. Overflow Characteristics in the DOME and the FBC Models

[7] Similar simulations were conducted for the five experiments described above, starting from initial conditions with source waters only at the locations indicated in Figure 3. After about 40 days in the DOME case and 60 days in the FBC cases the bottom plume waters propagated westward (and downslope, while mixing with the overlying waters) and reached the western open boundary. A radiation open boundary condition allows the plume and surface eddies to exit the domain with minimum reflections. Nevertheless, only results away from the boundary are analyzed. In the open ocean side of the domain there is no real steady state solution since eddies continue to be formed and propagate westward indefinitely (see later). However, after the initial adjustment period the statistics of mean properties do not change anymore (e.g., area averaged eddy kinetic energy calculated over days 30–40, 40–50 or 50–60 are similar).

[8] The structure of the bottom plume and the mixing properties in the DOME simulations with a 2.5 km grid size have been described in detail by *Ezer* [2005]. Therefore the main characteristics of the FBC simulations are first described before comparing the different experiments. Figure 4 shows the temperature structure across the channel and along the center of the channel in the intermediate sill width case, FBC-40. Note how the initial horizontal thick source water in the wide eastern side of the channel transformed into a tilted asymmetric layer (to form a geostrophically adjusted flow) as it approaches the narrow sill. Downstream of the Faroe Bank sill the overflow waters spread along the slope to form a much thinner and wider dense bottom plume that propagates westward and downslope. The structure of the simulated overflow shown in Figure 4 is in general, in good agreement with *Mauritzen et al.* [2005] (e.g., Figure 2) and other previously cited observations, though there are some differences. In particular, the observations show more spatial and temporal variations associated with small-scale topographic features and with upstream forcing variability, both effects are neglected in the idealized model. Another model deficiency is the structure in the sill itself (Figure 4d), which does not produce that well the pinching/spreading of isotherms along the south/north slopes (Figure 2, section D); this has been an observed characteristic for a long time and a subject of much discussion in the literature [*Saunders*, 1990; *Johnson and Sanford*, 1992; *Borenäs et al.*, 2001; *Borenäs and Lundberg*, 2004; *Lake et al.*, 2005]. The latest issue will be addressed later, when analyzing the details of the FBC-20 case which seems to produce this feature better than the FBC-40 or FBC-80 cases. Note that while the observed along-channel section (Figure 2, section I) does not extend as far away west of the sill as the model does, it does show some large variations in the 8°C isotherm that may relate to eddies as seen in the model (Figure 4g).

[9] To look at the time-dependent nature of the FBC model flow, the variations of the bottom plume structure and velocity 150 km downstream from the sill are shown in Figure 5 (see Figure 3b for the location of this section). A striking feature is the regular oscillatory behavior of the plume structure and velocity (Figures 5a and 5b). Observations taken 140 km downstream from the FBC sill reveal very similar oscillations [e.g., *Høyer and Quadfasel*, 2001, Figure 1; *Geyer et al.*, 2005]. The observed period of oscillation is ~3.5 days (compared with ~5 days in the model); the observed across-slope velocity fluctuations are $<\sim 0.3$ m s^{-1} ($<\sim 0.2$ m s^{-1} in the model); the observed along-slope velocity fluctuations are ~ 0.5 m s^{-1} (~ 0.3 m s^{-1} in the model); the observed bottom temperature fluctuations are 2°C–3°C (2°C–3°C in the model). Compared with the model oscillations, the observed fluctuations are more irregular and described as "a train of meso-scale eddies" [*Høyer and Quadfasel*, 2001]. The upslope/downslope meandering of the bottom plume in the model (Figures 5c and 5d) correlates with the oscillation of the along-slope flow (Figure 5a); pulses of maximum velocity occur when the bottom plume stretches further upslope over steeper topography (owing to the parabolic shape of the bottom). The along-slope velocity fluctuations can be explained by the theoretical propagation speed of eddies on a slope [*Nof*, 1983] given by $U_E = g'(s/f)$, where s is the bottom slope, f the Coriolis parameter, $g' = g(\Delta\rho/\rho_o)$ the reduced gravity, and $\Delta\rho/\rho_o$ the eddy's density anomaly relative to the background density. In this region in the model $g' \approx 5 \times 10^{-3}$ m s^{-2}, $f = 10^{-4}$ s^{-1}, and the slope at the center of the plume changes from $s_d = 0.009$ (the most downslope location) to $s_u = 0.015$ (the most upslope location); thus $U_u \sim 0.75$ m s^{-1} and $U_d \sim 0.45$ m s^{-1}. The difference in velocity according to theory is $U_u - U_d = 0.3$ m s^{-1}, which is exactly the range of change in the fluctuating velocity in the model. During the entire cycle, the flow is still supercritical since the actual velocity (0.99–0.71 m s^{-1}, Figures 5c and 5d) is larger than the gravity wave propagation speed (which is close to the Nof's velocity). Note also that when the plume is in its upslope position the entire transport associated with the plume increases and the return transport above the plume decreases.

[10] While the model and the observed oscillations resemble to some degree the oscillatory behavior of dense eddies on a constant slope as described by the analytical frictionless model of *Nof* [1984], the oscillations in the FBC have larger amplitude and lower frequency compared with the *Nof*'s [1984] analytical model (where the oscillations are at the inertial period). Unlike the frictionless oscillations proposed by *Nof* [1984], a mechanism of frictional destabilization in supercritical overflows may generate downslope propagating waves as suggested by *Swaters* [2003]. The exact mechanism of the observed and model oscillations is still not clear and beyond the scope of this study, though the model comparisons with the laboratory overflow experiments of *Cenedese et al.* [2004] in section 3.2 shed some light on the nature of these oscillations.

[11] After describing some of the typical characteristics of the FBC simulations, it is time to see how the FBC simulations are compared with previous DOME simulations. Figure 6 compares the surface elevation and velocity and the bottom tracer and velocity in the DOME and FBC-40 cases, near the time when the bottom plume reached the

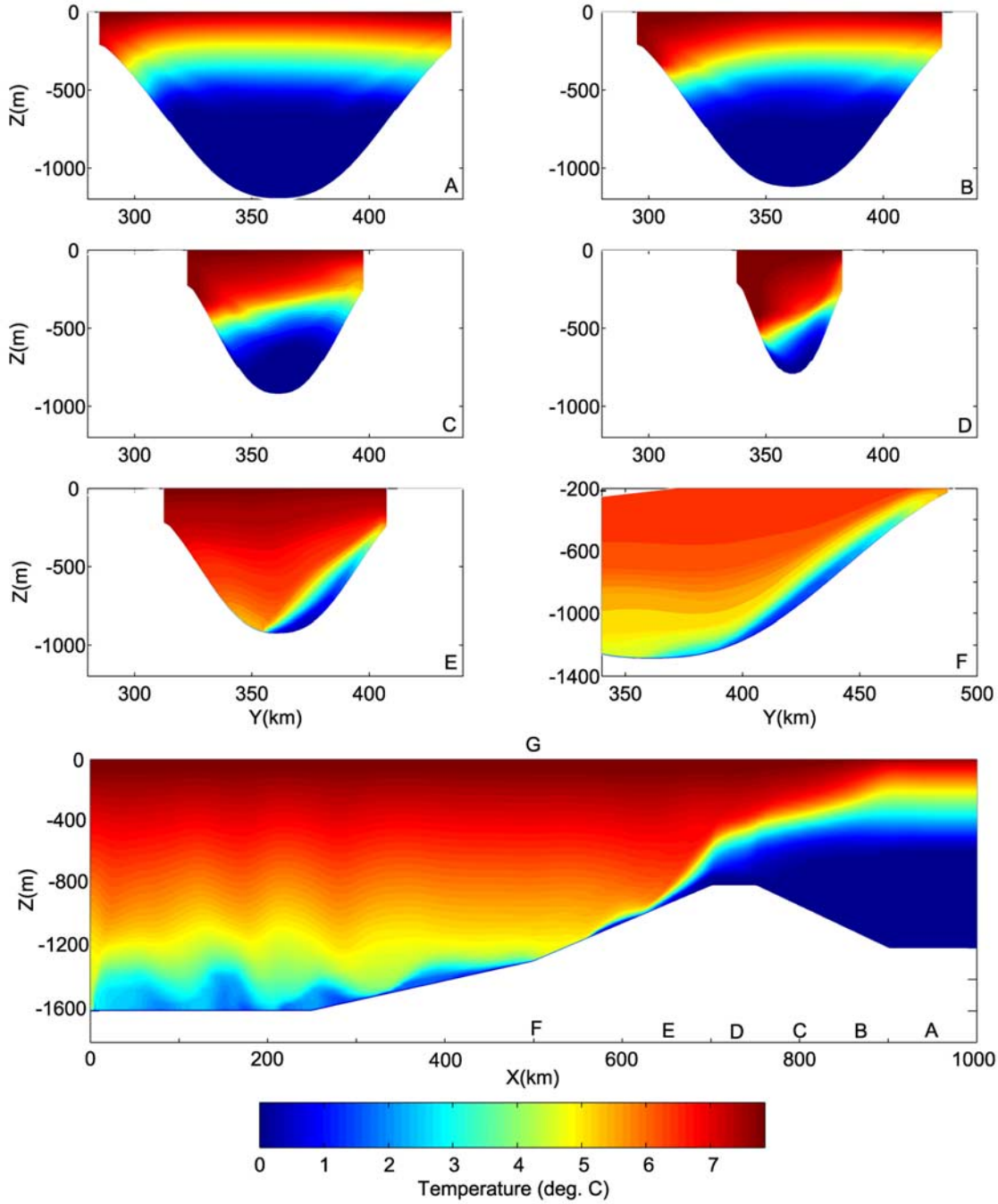

Figure 4. Model temperature after 60 days (FBC-40 case): (a–f) north-south sections across the channel and (g) east-west section along the center of the channel. The locations of the cross-channel sections are indicated in Figure 4g.

western boundary. The tracer concentration in the bottom plume indicates a significant difference in mixing between the two cases (Figures 6b and 6d). In the DOME case most of the entrainment occurs within 100–200 km from the sill [*Girton and Sanford*, 2003; *Ezer*, 2005; *Legg et al.*, 2006] causing a significant dilution of the plume, so that west of x = 700 km in Figure 6b an almost homogeneous, ~200 km wide, diluted plume is seen (with additional eddy mixing affecting regions farther downstream from the sill). In the FBC case, on the other hand, the plume is narrower and the mixing occurs over a much longer distance downstream from the sill. The signature of the bottom plume can be seen as surface eddies with diameter of ~50 km and ~10–15 cm surface elevation anomaly. Note however, that eddies in the DOME case are more frequent (typical periods ~2–3 days, Figure 6a) than eddies in the FBC case (typical periods ~5–8 days, Figure 6d). Measurements of temperature and velocity fluctuations downstream from the sills indeed indicate shorter eddy periods of ~2.8 days in the DS and longer, ~3.5 days, in the FBC [*Høyer and Quadfasel*, 2001, Figure 2]. The irregularity of the eddies in the FBC simulations may be attributed to stronger baroclinic insta-

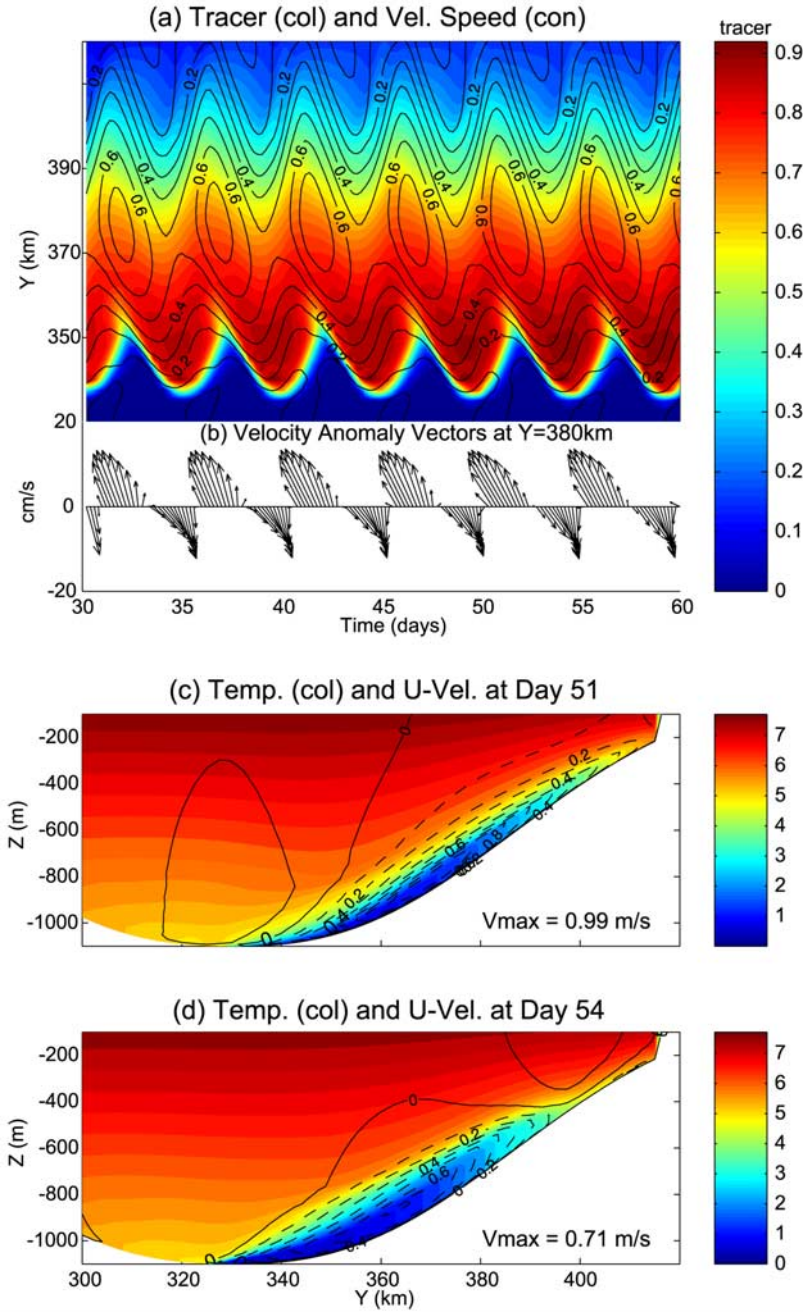

Figure 5. Time-dependent nature of the overflow 150 km downstream from the sill in the FBC-40 case (see location of the section in Figure 3b). (a) Bottom layer tracer concentration (red/blue colors represent source/ambient waters) and velocity (0.1 m s^{-1} contour interval) as a function of time for days 30–60. (b) Velocity anomaly vectors (relative to the 30-day mean) near the location of maximum velocity. (c) Examples of temperature (color) and along-slope velocity (dashed/solid contours represent flows toward the west/east) cross sections for day 51. (d) Same as Figure 5c but for day 54.

bility owing to the sharper bottom plume's front, as it is less diluted than the plume in the DOME case. Observations south of the Denmark Strait and numerical models indicate that surface mesoscale variability and eddies (~30 km in size) in the region may relate to variations in the overflow bottom plume [*Bruce*, 1995; *Krauss*, 1996; *Jiang and Garwood*, 1996; *Krauss and Käse*, 1998; *Spall and Price*, 1998; *Jungclaus et al.*, 2001; *Käse et al.*, 2003], in agreement with our model results (Figure 6a). Evidence for the existence of surface eddies associated with the FBC overflow is much more sparse, though analysis of altimeter data indicates significant enhancement of surface eddy kinetic energy and sea level variability downstream from the FBC sill [*Høyer and Quadfasel*, 2001]; our own analysis of altimeter data (shown later) further supports the findings of Høyer and Quadfasel.

[12] To summarize the influence of the overflow waters on water mass formation within the model domain, a useful

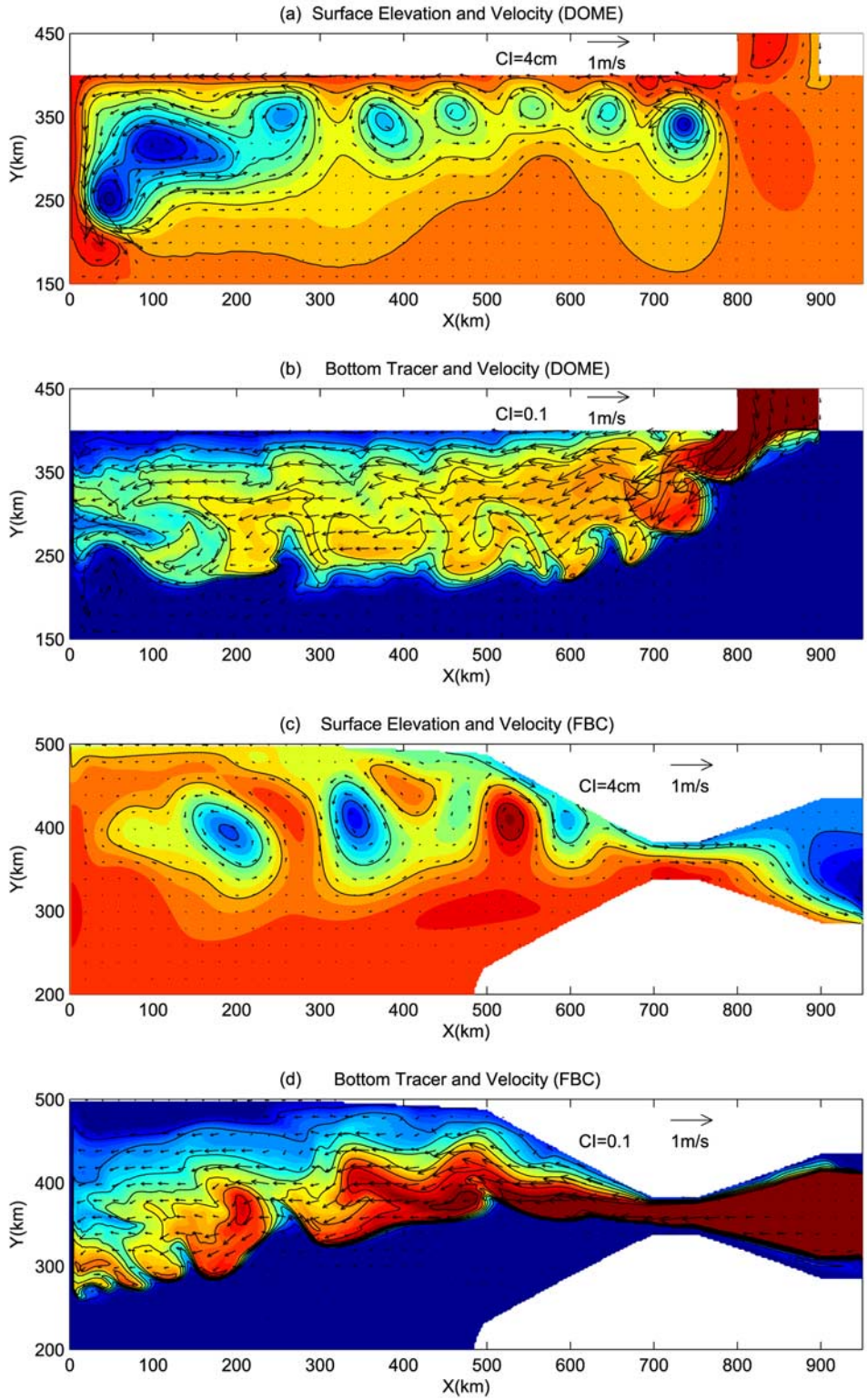

Figure 6. Instantaneous model fields (at 40 and 60 days in the DOME and the FBC-40 models, respectively): (a and c) surface elevation and surface velocity for the two models (contour interval is 4 cm and blue/red tones represent negative/positive values) and (b and d) bottom tracer concentration and bottom velocity for the two models (contour interval is 0.1 and blue to red tones represent values in the range 0–0.9).

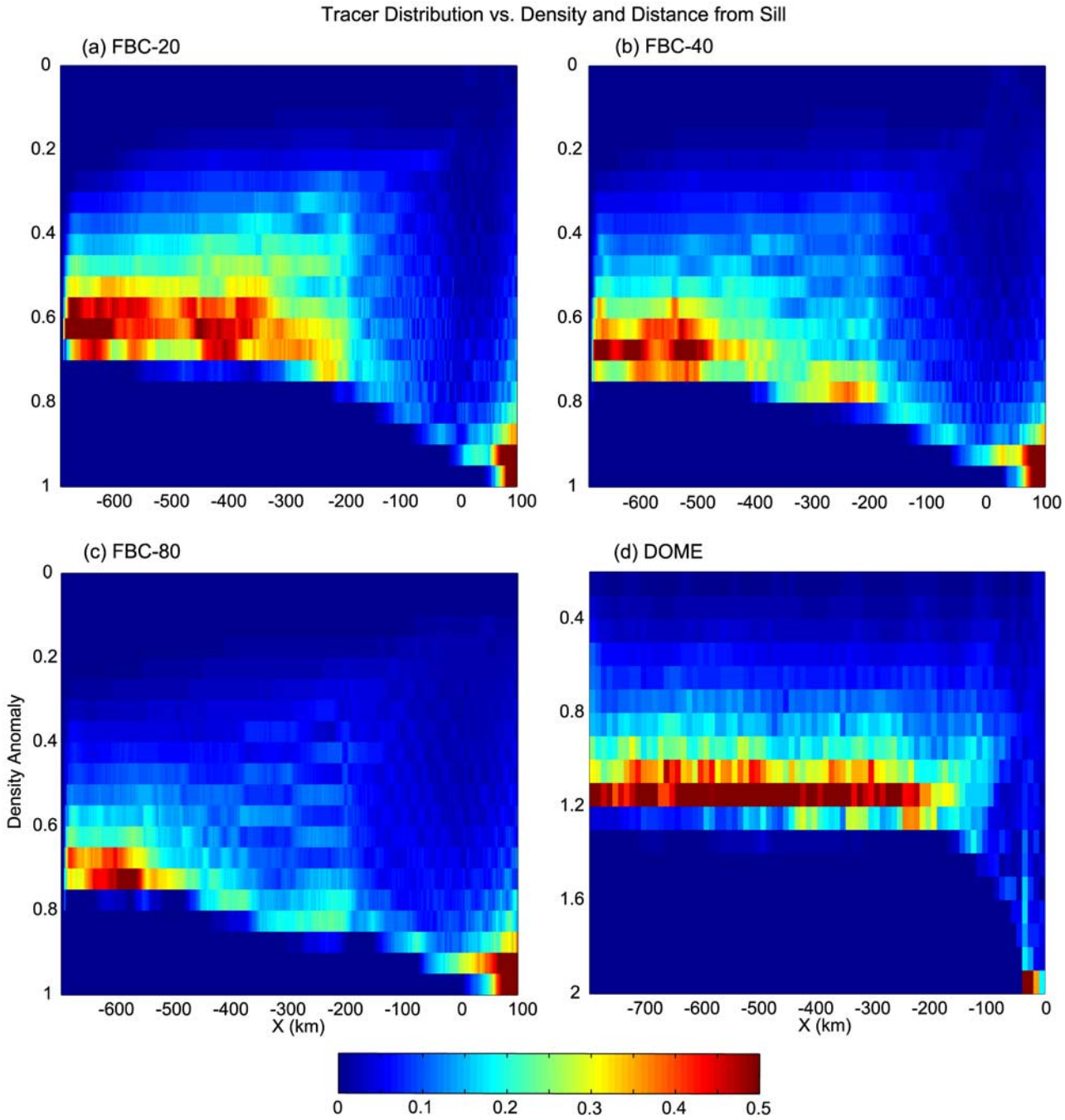

Figure 7. Histograms of the distribution of the north-south integrated tracer as a function of downstream distance, x, and density anomaly relative to surface open ocean density (vertical axis, units of kg m^{-3}) at the end of the (a) FBC-20, (b) FBC-40, (c) FBC-80, and (d) DOME simulations. The diagrams show how the source waters (red color near the bottom-right corner) settled at lower density levels as the plume mixes while propagating downstream. The blue regions near the bottom-left section of the diagrams represent deep layers without any trace of the source waters.

diagram (used also by *Ezer* [2005] and *Legg et al.* [2006]) is a histogram of tracer distribution as a function of downstream distance from the sill and density anomaly. (Density anomaly, in kg m^{-3}, is 0 at the surface and maximum at the deepest ocean and at the source.) Tracer values are normalized so that blue represents regions with no trace of the source water and red represents regions with high concentration of source waters. Figure 7 compares the water properties in the FBC cases (Figures 7a–7c) to the DOME case (Figure 7d), using the above diagram (note that in Figure 7 and the following figures x represents the distance from the sill not the distance from the model western boundary as in Figures 3–6). The diagram indicates that in the DOME case the source waters (located at the bottom-right corner of the diagram) are quickly mixed with overlying waters, so that it takes only 100–200 km for the

diluted source waters to settle at a neutral density level leaving large portion of the deep ocean unaffected by the overflow waters (the large blue region near the bottom half of Figure 7d). In the FBC cases on the other hand mixing and entrainment occur over a longer period, so that entrainment seems to halt only after 300, 400 and 600 km from the sill for the FBC-20, FBC-40 and FBC-80 cases, respectively (Figures 7a–7c). The mixing downstream from the sill is enhanced (i.e., the density of the overflow reduces faster with distance from the sill) when the sill in the model is narrower (i.e., the FBC-20 case) and more similar in size to the real sill width (~20 km). Observations do indicate enhanced mixing in the FBC [*Saunders*, 1990; *Duncan et al.*, 2003] with maximum mixing estimated around 100 km downstream from the sill [*Mauritzen et al.*, 2005]. What the sensitivity experiments demonstrate is that the narrow sill topography in fact causes the enhanced mixing in the FBC by enhancing frictional effects with the channel's walls and increasing shear (at least in the model). An interesting (and somewhat surprising) result is that, when the FBC is made artificially almost as wide as the DS sill is (Figure 7c), the results look most different than the DOME case (Figure 7d). The explanation is that the intense near-sill mixing in the (somewhat unrealistic) DOME configuration is caused by the abrupt encounter of the overflow waters on the wide and flat embayment with the sudden continental slope and warmer waters (may be fortuitously, an abrupt encounter of water masses in the DS causes similar strong mixing). It should be noted that despite some unrealistic features in the DOME configuration, the simulated structure of the bottom plume (Figure 6b) is actually compared quite well with the overflow plume simulated by models with realistic DS topography [e.g., *Käse et al.*, 2003, Figure 1]. In the FBC configuration on the other hand, the flow is geostrophically adjusted in the upstream channel (with a return flow in the upper layer) so that the encounter between the overflow and the waters of the open ocean is not as brief as in the DOME case; mixing and entrainment are caused by processes such as bottom turbulence, diapycnal mixing and eddies along the long path of the plume.

3.2. Eddies, Waves, and Downstream Dynamics in the FBC

[13] In this section, a more detailed analysis of the FBC cases will be conducted in order to study the effect of the sill topography on the characteristics and dynamics of the downstream variability. Two important parameters that characterize the stability and dynamics of geophysical flows and overflows in particular [*Cenedese et al.*, 2004], are the Ekman number, $Ek = (\delta/h)^2$, where δ is the Ekman layer thickness and h is the plume thickness, and the Froude number, $Fr = \Delta U/\sqrt{g'h}$, where ΔU is the velocity difference between the upper and bottom layers, and g' the reduced gravity. Figure 8 shows the distribution of Fr, g', ΔU and h in the FBC-40 model (the other FBC cases are qualitatively similar in nature). In the "upstream region", between the source and the sill, the Froude number is very small, $0 < Fr < 0.2$, mostly due to the thick bottom layer, $h > 500$ m (Figures 4a–4c and Figure 8d), thus the flow is subcritical and quite stable. In the "downstream region", between the sill and the slope of the open ocean, the Froude number is very large (Fr > 1), since h becomes small as the plume spreads on the slope (Figure 4f) but ΔU is maximum there (Figure 8c) with plume velocities reaching 0.8–1 m s^{-1}, similar to the observed near-bottom velocities [*Saunders*, 1990; *Johnson and Sanford*, 1992; *Mauritzen et al.*, 2005]. In this region the Ekman layer (inferred from velocity profiles) is comparable or slightly smaller than the plume thickness (Figures 5c and 5d), so the Ekman number is around 0.1–1. The laboratory overflow simulations of *Cenedese et al.* [2004] show that under supercritical conditions with $Fr \geq 1$ (and $0.05 < Ek < 5$) the flow is in a "wave regime" where "blobs" of dense bottom plume propagate at an almost constant speed in the same direction as the bottom plume. In the third, "open slope" regime, west of the end of the channel, the bottom velocity (and thus ΔU) is reduced faster than the reduction of g', so that typically $0.4 < Fr < 0.6$ and $0.01 < Ek < 0.1$. This range of the Froude number (and $Ek < 0.1$) is exactly the "eddy regime" in the laboratory overflow experiments of *Cenedese et al.* [2004]. The mechanism that creates cyclonic eddies in overflow regions involved breakup of eddies from the unstable plume and the conservation of potential vorticity [e.g., *Spall and Price*, 1998]. For comparison, in the model simulations with the DOME domain, $0.4 < Fr < 0.6$ almost everywhere, except inside the embayment where $Fr \leq 1$ is imposed [*Ezer*, 2005]. The behavior of the flow past the FBC sill in the model resembles to some degree the classic hydraulic controlled frictional channel flow over a sill [*Pratt*, 1986]. However, the way the dynamics downstream is affected by the sill topography is not so simple, as shown next.

[14] Figure 9 shows the bottom transport (in four FBC experiments, three different sill widths and one with no background stratification) as a function of distance from the sill and time (the so-called "Hovmöller diagram" is useful to identify propagating signals). Three different flow regimes are clearly seen in the simulations, in accordance with the flow regimes described by the Froude number (they are marked on the top of Figure 9a). In the upstream channel where the flow is subcritical, except a uniform small increase in transport (i.e., entrainment), there are almost no time-dependent variations. (Observed flow variations there, as seen in the work by *Mauritzen et al.*, 2005, are probably due to external forcing.) The downstream supercritical region is characterized by a "wave" solution (as expected from Fr and *Cenedese et al.* [2004] lab experiments) with regular oscillations in transport. The strongest propagating signals are found in the "eddy" regime farther downstream, where irregular eddies are formed and are propagated westward. In the more realistic configurations (Figures 9a and 9b) there seem to be a clear distinction between the "wave" and the "eddy" regimes which have different timescales. In the wide-sill case (Figure 9c) and in the case with no stratification (Figure 9d) such distinction in timescales is not so clear. The background stratification and the narrow FBC sill seem to play crucial roles in the downstream dynamics, affecting eddy intensities, eddy periods and propagation speed. (Note that different contour intervals are used in each plot in Figure 9). The lack of background stratification (thus larger g') causes eddies to intensify by a factor of two, despite the fact that transport in the sill itself is almost unaffected by the background stratification (comparing Figures 9b and 9d). Comparing

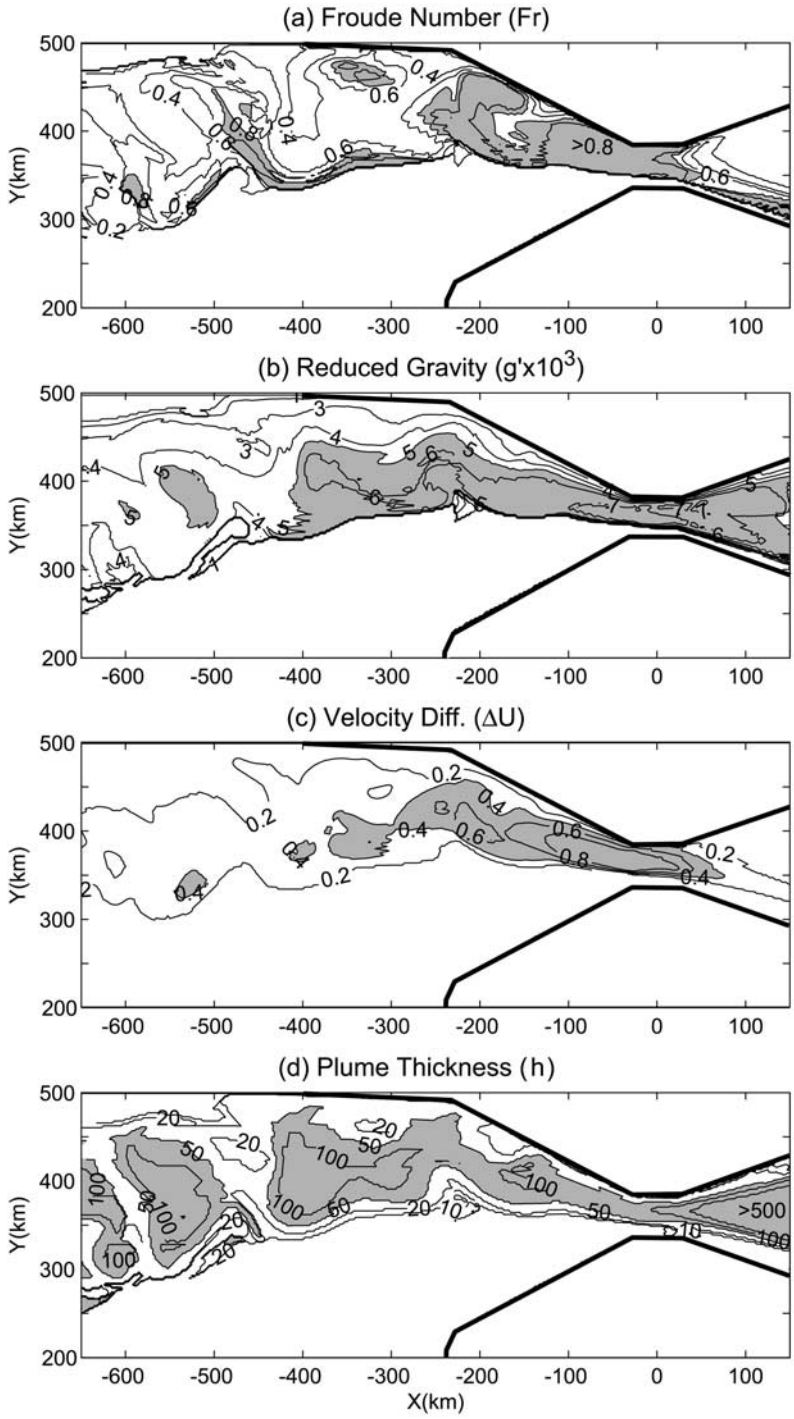

Figure 8. Mixing properties of the FBC-40 bottom plume: (a) Froude number, $Fr = \Delta U/(g'h)^{1/2}$ (contour interval is 0.2, and shaded regions represent $Fr > 0.8$), (b) reduced gravity, $g' = g\Delta\rho/\rho_o$ (contour interval is 10^{-3} m s^{-2}, and shaded regions represent $g' > 5 \times 10^{-3}$ m s^{-2}), (c) velocity difference, ΔU, between overlying water velocity and bottom plume velocity (contour interval is 0.2 m s^{-1}, and shaded regions represent $\Delta U > 0.4$ m s^{-1}), and (d) bottom plume thickness, h (contours are shown for h = 10, 20, 50, 100, 200, and 500 m, and regions with $h > 50$ m are shaded).

Figure 9 with a similar Hovmöller diagram obtained from the DS model of *Käse et al.* [2003] indicates that strong pulses of transport propagating downstream in the DS case can be seen only up to ~150 km from the sill, a possible result of the intense mixing near the DS sill as discussed before.

[15] Figure 10 shows the mean and standard deviation of the bottom transport (negative values imply westward flows) as a function of the distance from the sill. The sill transport in the FBC-20 case, 2.5 Sv, is only slightly larger than observed (though transports may vary between 1 and 3.5 Sv [*Mauritzen et al.*, 2005]). The transport continues

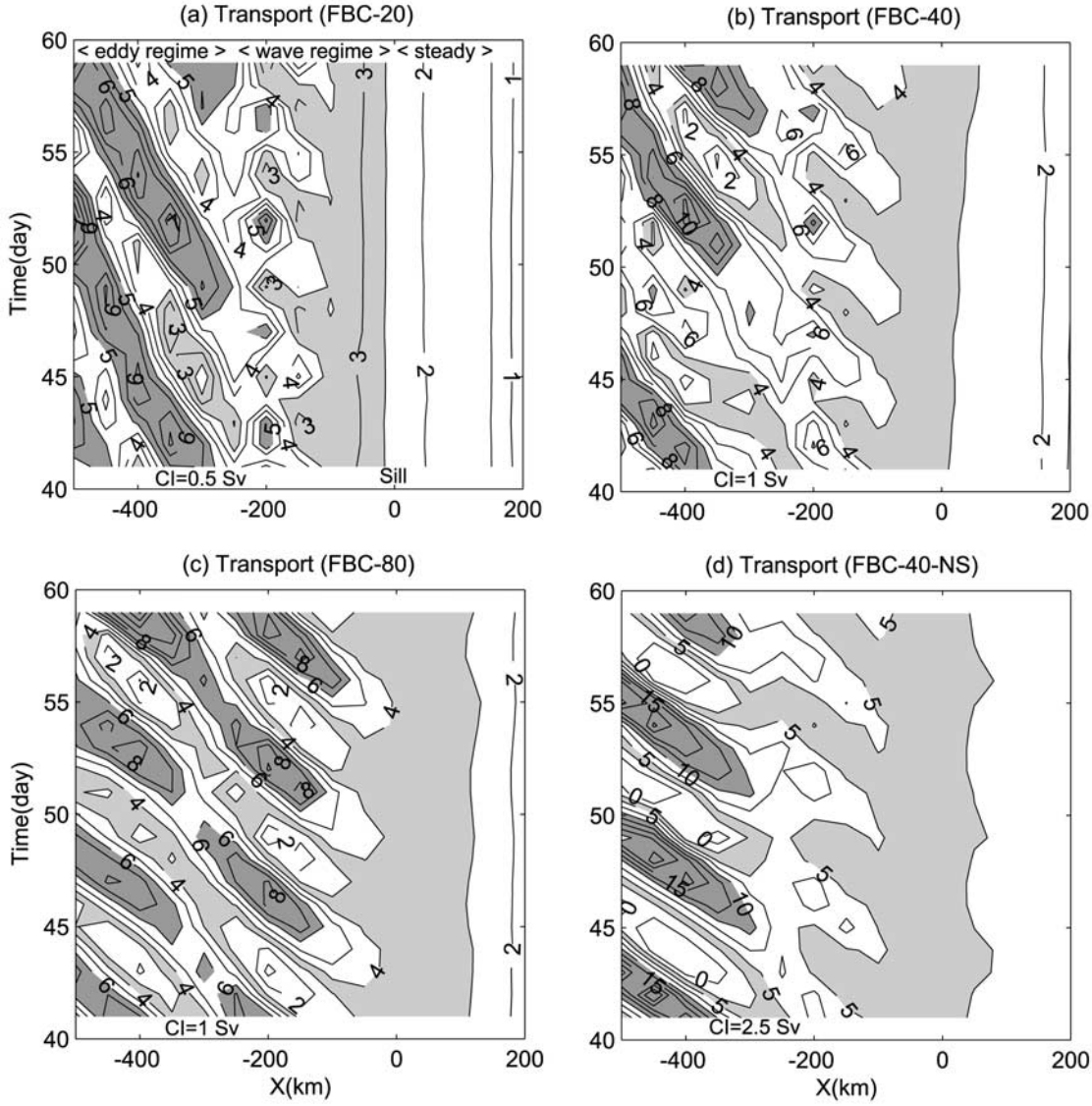

Figure 9. Bottom plume transport as a function of downstream distance from the sill and time (days 40–60) for simulations (a) FBC-20, (b) FBC-40, (c) FBC-80, and (d) FBC-40-NS. Note the different contour interval in each plot. All values are negative (westward transports), so negative signs were ignored in the contour labeling. Dark shades highlight large transports associated with eddies, and light shades represent mostly the ''wave regime'' (see text).

to grow (indicating entrainment) throughout the domain in all cases, though the mean eddy transport 500 km from the sill (~5–7 Sv) does not seem to be too sensitive to the sill width. As seen in Figure 9, a clear distinction between the variability in the ''wave'' and the variability in the ''eddy'' regimes is evident in the model. The variability in the ''wave'' regime is increased when the sill width is increased because of the decreasing in mixing (Figure 7) and thus increasing in g'. On the other hand the variability in the ''eddy'' regime is most affected by background stratification (Figure 10d). A comparison of propagation speeds and periods between the different cases is summarized in Figure 11. Note that since the propagation speed of bottom eddies and plumes on a sloping bottom very closely follows the *Nof*'s [1983] relation, $U_E = g'(s/f)$, both in models [*Ezer*, 2005] and in laboratory experiments [*Cenedese et al.*, 2004], the *y axis* in Figure 11 is approximately equal to g' when multiplying the velocity values by a factor of 0.01. The enhanced mixing due to the narrow sill decreases the propagation speed (and thus plume density) by a factor of two compared with the FBC-80 case. In fact, in the cases with no background stratification or with a very wide sill, the sill topography plays only a minor role in the mixing process. The small increase in the eddy speed compared to the wave speed in the FBC-80 case is explained by the slight increase in bottom slope. Note that unlike the wave propagation speed, the wave period (~4.5–6.5 days) is only weakly dependent on the sill topography and seems to be controlled by the supercritical flow and bottom friction effects (*Mauritzen et al.* [2005] found maximum frictional stress about 150 km downstream from the sill).

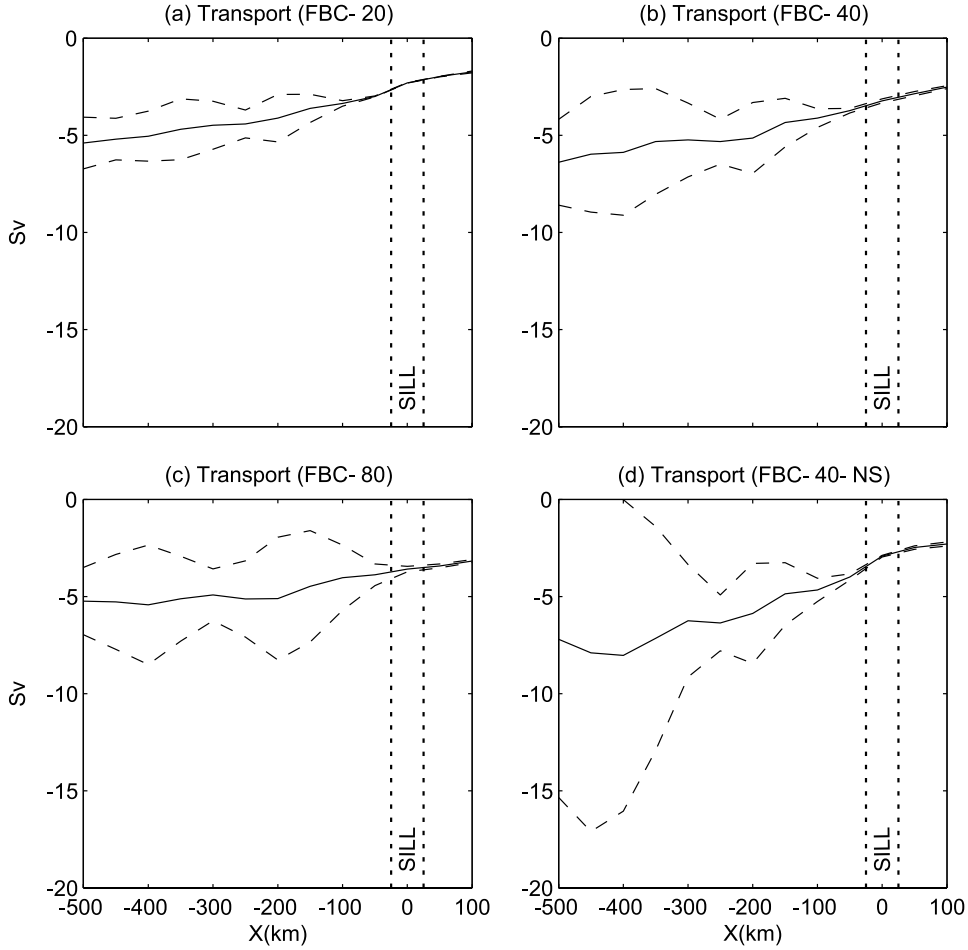

Figure 10. Mean (solid line) and standard deviation range (dashed lines) of transport as a function of distance from the sill calculated from days 40–60 for cases (a) FBC-20, (b) FBC-40, (c) FBC-80, and (d) FBC-40-NS.

[16] As to observed oscillations, *Saunders* [1990] analyzed current meter moorings in the FBC and found a "striking" time dependence oscillations with 3–6 days period in the warm water above the overflow; after considering several mechanisms such as seiches and Kelvin waves he concludes: "the origin and nature of these motions remains unknown". Since then numerous other studies described oscillations with similar periods in the bottom plume downstream from the sill [*Borenäs and Lundberg*, 2004; *Høyer and Quadfasel*, 2001; *Geyer et al.*, 2005]; these oscillations are generally found in the region defined here as the "wave" regime. The model calculations (Figures 5 and 9–11) show that such variations are persistent features of the FBC overflow, though quantitatively the period and propagation speed may be affected by the detailed topography of the sill. Since no external time-dependent forcing exists in the model, these variations are excited internally when the flow is supercritical, but are not forced externally by variations in the sill itself.

3.3. Observed Surface Eddies and the FBC Overflow

[17] While there are many studies that indicate a relation between the mesoscale surface variability downstream from the DS sill and variations in the deep overflow [*Bruce*, 1995; *Krauss*, 1996; *Jiang and Garwood*, 1996; *Krauss and Käse*, 1998; *Spall and Price*, 1998; *Jungclaus et al.*, 2001; *Käse et al.*, 2003], there were only few attempts to detect the effect of the FBC overflow on surface variability. Small gradients in Sea Surface Temperature (SST) near the FBC region make it difficult to detect FBC eddies (if they exist) from satellite SST images. However, *Høyer and Quadfasel* [2001] analyzed altimeter data in the FBC region and found significant enhancement of surface eddy kinetic energy and sea level variability, with maximum variability detected ~30 km downstream from the FBC sill. Model results (Figure 10) indicate enhanced bottom variability downstream from the sill. Surface eddies associated with the bottom plume (Figure 5) have a sea surface height signature of about 10 cm; such signal may be detected by satellite altimetry data.

[18] Examples of sea surface height anomalies obtained from optimally combining TOPEX/Poseidon and ERS satellites [*Ducet et al.*, 2000] in 10 days intervals are shown in Figure 12. During this 1-month period (and other periods not shown) there is an indication of negative anomalies that seem to propagate along the north side of the channel. One anomaly (marked "A") is first seen at ~100 km downstream from the sill (the sill is located around 8°W, 61.3°N) and propagated northwestward along the slope. Another negative anomaly upstream of the sill (about twice as strong

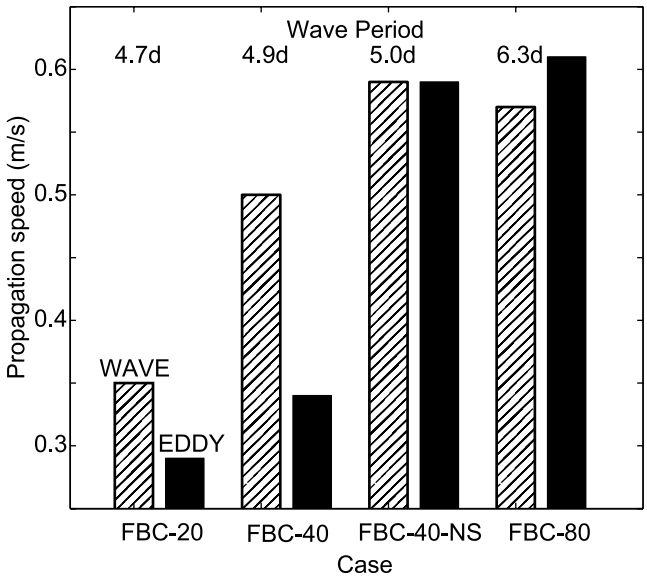

Figure 11. Estimated propagation speed of "waves" (hatched bars) and "eddies" (solid bars) for the four FBC experiments (see Figure 9); wave period is also indicated. Note that because of the Nof's eddy speed relation, the y axis (U in m s^{-1}) is approximately proportional to reduced gravity, g' (m s^{-2}) $\approx 0.01\ U$.

as eddy "A" and marked "B") is seen in the east part of the channel (at the Faroe-Shetland Channel). Eddy "B" propagates southwestward toward the sill, but as seen in many other periods (not shown) the large anomaly has difficulty negotiating the strong curvature and the narrowing of the channel, creating a semipermanent eddy between 4°W–6°W. This anomaly is quite similar to the one seen in the model around x = 900 km in Figure 6c. Surface cyclonic flow at almost the exact location as eddy "B" has been seen also from direct observations [*Mauritzen et al.*, 2005, Figure 5] and from drifters and altimeter data [*Sherwin et al.*, 1999]. While the upstream Faroe-Shetland Channel is known to have considerable mesoscale variability, more work is clearly needed to verify the enhanced surface variability downstream from the FBC sill and its relation with the overflow variability as suggested by *Høyer and Quadfasel* [2001] and by our analysis.

3.4. Cross-Channel Dynamics in the FBC Sill

[19] Observations across the narrow FBC sill region have shown several interesting features. Some are quite well understood, such as the strong upward tilt of isopycnals from south to north which is consistent with the geostrophic adjustment of the flow in the channel. Other features, such as time-dependent variations in the overflow structure and transport, that may relate to atmospheric forcing or upstream variations are not fully understood yet [*Mauritzen et al.*, 2005]; these variations will not be addressed here. One intriguing feature that is seen consistently in most observations (e.g., Figure 2, section D) is the asymmetry in the isotherms across the channel; the isotherms often pinched at the southern wall of the channel and spread toward the northern wall of the channel [*Borenäs and Lundberg*, 1988, 2004; *Saunders*, 1990; *Johnson and Sanford*, 1992; *Borenäs et al.*, 2001; *Lake et al.*, 2005]. On the basis of observed velocity profiles, *Johnson and Sanford* [1992] suggest the following mechanism to explain the thermal structure: The strong stress at the bottom boundary layer creates a southward cross-channel flow and upwelling near the southern wall which causes the pinching of isotherms there, while the isotherms are spread by interfacial mixing when the cross streamflow returns northward along the interface. *Borenäs et al.* [2001] on the other hand, offered an alternative mechanism for the isopycnal pinching, on the basis of inviscid hydraulic adjustment theory proposed by *Hogg* [1983]; this mechanism involves an additional intermediate water mass, which is sometimes found in the FBC. However, *Borenäs et al.* [2001] conclude that the data cannot unambiguously support one theory over the other, and that both mechanisms may play some role in the FBC dynamics.

[20] While the idealized model does not have intermediate water mass to test the *Borenäs et al.* [2001] mechanism, we should be able to see to what extent the model results support *Johnson and Sanford*'s [1992] mechanism. Figure 13 thus show the thermal structure, the along channel flow, the across channel circulation and mixing coefficient calculated by the Mellor-Yamada turbulence scheme (for the FBC-20 experiment). The flow in the narrow channel reaches almost a steady state after the initial adjustment, so after say 10 days no significant variations are seen (without external forcing). It is noted first that the northward (from left to right) spreading of the isotherms (Figure 13a) is much more realistic here than in the FBC-40 (Figure 4d) case, indicating the important role played by the narrow channel in maintaining this structure. The along-channel flow (Figure 13b) shows a two-layer flow with a westward (negative U) outflow, mostly below 400 m, and a return flow in the upper layers above. While the maximum deep flow (>0.8 m s^{-1}) and upper flow (>0.4 m s^{-1}) values are in general good agreement with observations [e.g., *Mauritzen et al.*, 2005, Figure 9] there are differences in details. For example, the maximum observed return flow is often found in the center or the southern side of the channel, while in the model it is found on the northern side (the model idealized configuration requires all the return flow to be in the channel while in reality return flows can occur in other passages and shallow banks). The across-channel circulation (Figure 13d) shows two main circulation cells. The bottom cell (indicated by dashed contours) is driven by the southward Ekman flow in the bottom boundary layer (where the westward outflow veers to the left when approaching the bottom) and then flow returns north and upward, about 200 m above the bottom. In the top cell the return eastward upper flow, which is stronger near the surface (Figure 13b), veer to the right (like an Ekman surface layer) causing a southward cross-channel flow in the upper 200 m. The result of this cross-channel circulation is a convergence zone along the southern slope (with upwelling from below and downwelling from above) which may explain the pinching of isotherms there. So far the model results are in full agreement with the bottom friction-driven mechanism proposed by *Johnson and Sanford* [1992]. However, the model results suggest that the mechanism responsible for the northward spreading of the isotherms is a little different than that proposed by Johnson and Sanford (they suggested that the northward flow along

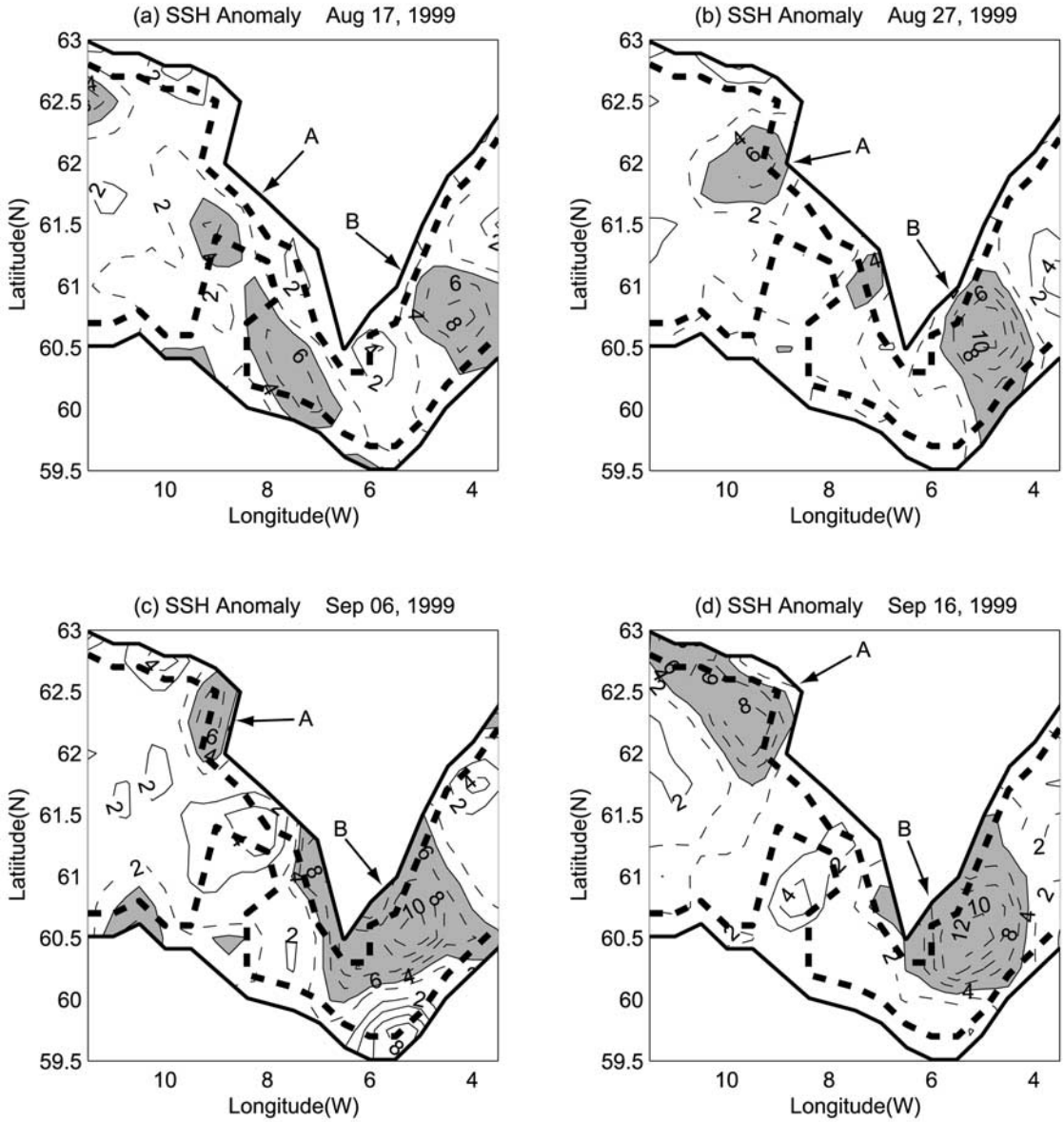

Figure 12. Sea surface height anomaly from satellite altimeter data (10-day composites 17 August to 16 September 1999) over the FBC region. Contour interval is 2 cm with dashed lines for negative values. The thick dashed lines roughly represent the edges of the channel; the deep flow (not shown) is from the right side of the domain, and the sill is at 8°W, 61.2°N. The shaded regions represent negative anomalies that seem to propagate along the north slope of the channel: Anomaly marked "A" is downstream of the sill, and anomaly marked "B" is upstream of the sill in the Faroe-Shetland Channel.

the isotherms undergoes mixing due to the high shear in the interface region). Laboratory experiments of frictional rotating hydraulic channel flows by *Johnson and Ohlsen* [1994] also show a cross-channel flow similar to the model (their Figure 5 resembling Figure 13d), though they suggest that the upper southward flow is the return of the northward flow driven by the interfacial friction and not due to the surface return flow as suggested here; in reality both mechanisms may play a role. In the model, the downwelling along the two slopes results in upwelling in the center of the channel (which becomes stronger on the north side where stream function contours are tighter). This upwelling will tend to lift and spread the isotherms (i.e., the across-channel northward flow is not exactly along the isotherms, but has a significant across-isotherm component). In addition, the downslope Ekman bottom flow along the northern slope will tend to push the lower isotherms downward, further spreading them. The mixing coefficient structure (Figure 13c) does not show strong vertical mixing along the interface in the middle of the channel (as suggested by Johnson and Sanford's mechanism) despite the high shear there. The stable stratification across the interface seems to restrain development of turbulence there (at least that is what the turbulence scheme produces given the model vertical grid resolution which is higher, $\sim$1 m, near the bottom but only $\sim$10 m near the interface). Though the model vertical

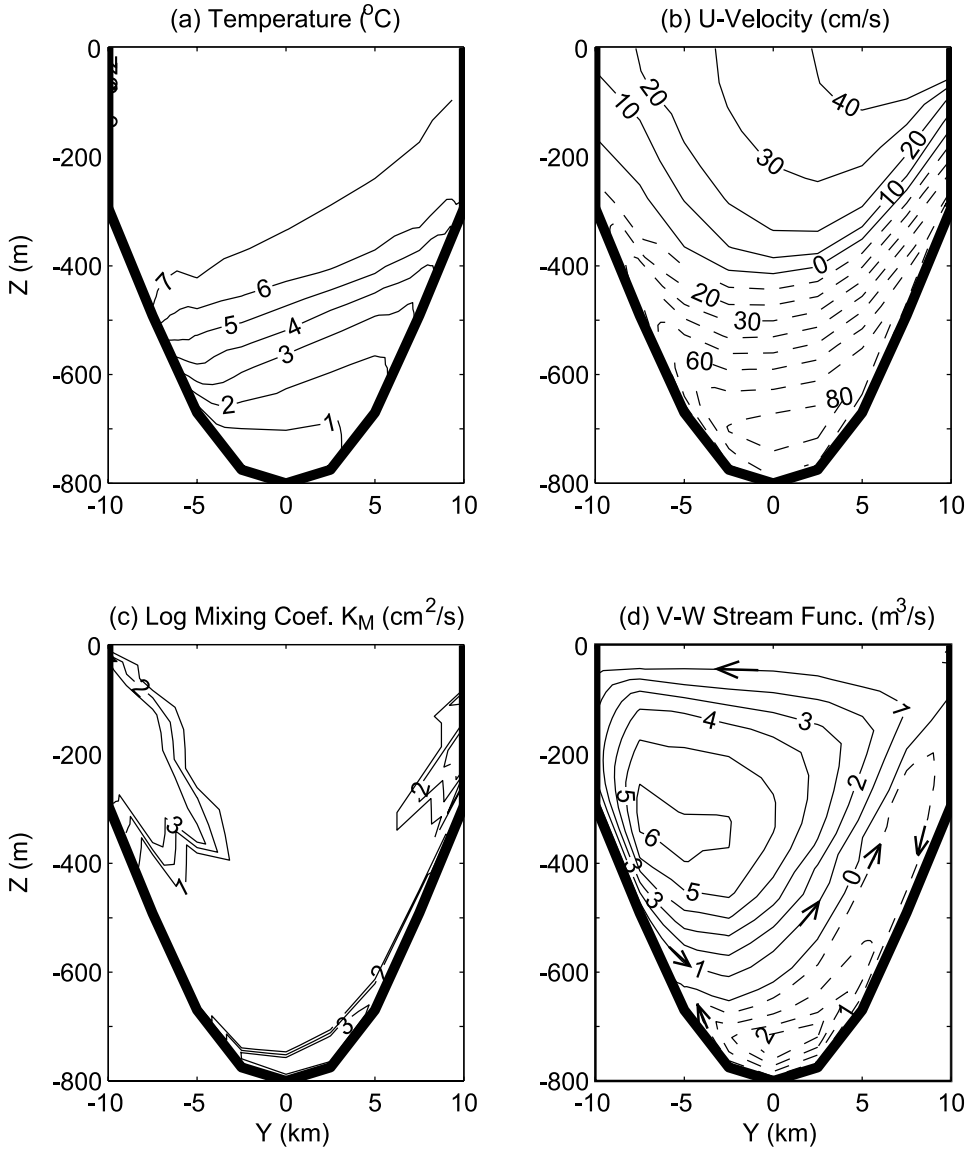

Figure 13. Cross sections at the center of the sill (experiment FBC-20) of (a) temperature, T (°C); (b) along-channel velocity component, U (cm s^{-1}); (c) log of the turbulent mixing coefficient K_M (cm^2 s^{-1}); and (d) across-channel stream function Ψ (m^3 s^{-1}) representing the V and W velocity components ($V = \partial\Psi/\partial Z$, $W = -\partial\Psi/Y$).

resolution may not allow detailed analysis of the dynamics across the interface (this may also require nonhydrostatic models), cross isotherm advection may create buoyancy flux convergence due to mixing there.

[21] The vertical mixing produced by the Mellor-Yamada turbulence scheme (Figure 13c) indicates large values of $100-1000 \times 10^{-4}$ m^2 s^{-1}. Enhanced overflow mixing of that magnitude has been estimations based on observations [*Saunders*, 1990; *Duncan et al.*, 2003; *Mauritzen et al.*, 2005]. However, the enhanced mixing in the model is limited to three regions, two of them along the upper walls of the channel, and one in the bottom boundary layer (BBL). The downwelling along the upper walls destabilizes the stratification and creates strong mixing there (though enhanced mixing has little effect on the southern upper wall where waters are quite homogeneous anyways). The bottom boundary layer thickness of ~30 m in the center of the channel is in good agreement with the observations of *Johnson and Sanford* [1992]. The (downslope) Ekman transport on the northern slope tends to create a thick mixed layer there (seen in Figure 13a) while the (upslope) Ekman transport on the southern lower slope tends to create more stably stratified layers there (i.e., the pinching). This BBL asymmetry across dense plumes on sloping bottoms is a typical feature in models and observations [*Ezer and Weatherly*, 1990; *Ezer*, 2005], and seems to create a more diluted upslope front and a sharper downslope front as clearly seen in the tracer distribution across the plume in Figure 5a.

4. Discussion and Conclusions

[22] Better understanding of the dynamics of overflows is important for climate and ocean circulation studies, since

the entrainment and mixing near few critical straits and sills may affect deep water mass formation throughout the world oceans. Unfortunately, typical coarse resolution climate and circulation models do not resolve those critical regions and thus relay on some simplifications or parameterizations for the unresolved scales. This shortcoming motivates research activities such as the Climate Process Team–Gravity Current Entrainment (CPT-GCE) initiative which brings together overflow studies based on observations [*Mauritzen et al.*, 2005; *Girton and Sanford*, 2003], laboratory experiments [e.g., *Cenedese et al.*, 2004] and various overflow models [*Ozgokmen and Chassignet*, 2002; *Papadakis et al.*, 2002; *Käse et al.*, 2003; *Ezer and Mellor*, 2004; *Ezer*, 2005; *Legg et al.*, 2006]; the results presented here are part of these efforts.

[23] The focus here is on one aspect of overflow dynamics: the influence that the local topography near the sill region has on mixing properties and the dynamics of the bottom gravity current. The study follows on the footsteps of previous idealized simulations that capture some characteristics of the Denmark Strait overflow using the so-called DOME (Dynamics of Overflow Mixing and Entrainment) configuration. While the idealized configuration has many unrealistic features, it allows to study mixing processes in a controlled environment, and provides an excellent benchmark to compare various models and mixing schemes [*Ezer and Mellor*, 2004; *Ezer*, 2005; *Legg et al.*, 2006]. Here, a modification in the DOME topography was introduced so that the sill area more closely resembles the conditions near the Faroe Bank Channel overflow region. A terrain-following ocean model with a 2.5 km horizontal grid size (a sufficiently fine grid to resolve the typical eddies in the bottom plume as shown by *Ezer* [2005] and *Legg et al.* [2006]) is used to compare between the previous DOME simulations and simulations with a FBC-like topography; sensitivity experiments with various sill widths (20, 40 and 80 km) and with no background stratification were also conducted. The sill topography in the model found to be vital to the overflow mixing and the downstream dynamics. The enhanced mixing observed downstream from the FBC sill [*Mauritzen et al.*, 2005] is linked here to the narrow channel and associated bottom friction and shears, whereas downstream mixing is significantly reduced in experiments with (unrealistically) wide FBC sill configurations. Enhanced mixing in the DOME configuration on the other hand, may relate to the abrupt encounter of water masses (and to some degree to the artificial DOME topography).

[24] Analysis of parameters that affect the dynamics such as the Ekman number (*Ek*) and the Froude number (*Fr*) indicates three different flow regimes, closely resembling the regimes found in the laboratory overflow experiments of *Cenedese et al.* [2004]. In the wide channel upstream of the FBC sill $Fr \ll 1$ and the simulated flow is subcritical and almost steady (observed variations in the Faroe-Shetland Channel upstream from the FBC are not simulated here). In the region between the sill and ~100–200 km downstream the flow is supercritical ($Fr \geq 1$), mixing and entrainment are strong, and the simulated flow is in what was called here a "wave" regime. In this region our model and observations [*Høyer and Quadfasel*, 2001; *Geyer et al.*, 2005] show near bottom temperature and velocity oscillations along the slope with periods of 3–6 days. Earlier observed oscillations in the warm waters above the FBC overflow with similar frequencies [*Saunders*, 1990] may be related to the overflow variations; the model indicates the oscillations can be detected throughout the water column. Enhanced sea level variability in this region has been detected from altimeter data [*Høyer and Quadfasel*, 2001]. Farther downstream, when the overflow plume has been further diluted and has slowed down its descent, $0.4 < Fr < 0.6$, and the overflow is in the so-called "eddy" regime. In this region irregular mesoscale surface eddies associated with variations of the bottom plume are seen propagating along the slope, similar to eddies previously found downstream of the DS [*Bruce*, 1995; *Krauss*, 1996; *Krauss and Käse*, 1998; *Jungclaus et al.*, 2001; *Käse et al.*, 2003]. Analysis of altimeter data (Figure 12) suggests that it is possible to detect the propagation of those eddies in the FBC region.

[25] The sensitivity experiments with various FBC sill width and stratification demonstrate how the downstream dynamics (e.g., wave propagation speed and period, eddy intensity and frequency, etc.) are affected by the sill configuration. When the model sill is narrow, and more closely resembles the real topography, the distinction between the different flow regimes is more pronounced than when the sill is artificially wide. Background stratification seems to limit the growth and descent of eddies in the "eddy" regime, but has little effect on the oscillations in the "wave" regime.

[26] Despite the fact that the model configuration is highly idealized and primarily meant to study the sensitivity of overflows to sill topography, and not to imitate reality in details, the basic observed characteristics of the Faroe Bank Channel overflow are simulated quite well. Idealized models can also help to study processes in a controlled environment, for example, an analysis of the cross-channel dynamics at the sill itself was conducted. The purpose was to investigate the peculiar structure of the observed isotherms across the channel [*Borenäs and Lundberg*, 1988; *Saunders*, 1990; *Johnson and Sanford*, 1992; *Borenäs et al.*, 2001]. The cross-channel model circulation confirms the observation-based mechanism proposed by *Johnson and Sanford* [1992] that Ekman driven flows in the bottom boundary layer causes upwelling along the southern slope and pinching of the isotherms there. However, interpreting the model results required a little twist in the proposed mechanism. The spreading of the isotherms across the channel from south to north was attributed in the model to the combined effect of upwelling across the isotherms in the middle of the channel and bottom mixing along the northern slope, and not due to shear-driven mixing at the interface as suggested by Johnson and Sanford.

[27] In summary, there are clearly issues that need further research before mixing processes in overflows are fully understood and accurately modeled; such issues include for example, the nature and forcing of high-frequency variation in the FBC and the effect of external forcing at the surface and the effect of upstream variability. Ways to parameterize overflow mixing in climate models is still an area of active research. A combination of analytical and numerical models (idealized, realistic, hydrostatic and nonhydrostatic) as well as field observations and laboratory experiments are now part of an ongoing collaborative research aimed to address those issues.

[28] **Acknowledgments.** This study is part of the Climate Process Team–Gravity Current Entrainment (CPT-GCE) project, supported by NSF award OCE-0336768. Additional support is provided by the Office of Naval Research (ONR), award N00014-04-10381. Two anonymous reviewers provided many useful suggestions. Computational resources were provided by NOAA/GFDL.

References

Adcroft, A., C. Hill, and J. Marshall (1997), Representation of topography by shaved cells in a height coordinate ocean model, *Mon. Weather Rev.*, *125*, 2293–2315.

Beckmann, A., and R. Döscher (1997), A method for improved representation of dense water spreading over topography in geopotential-coordinate models, *J. Phys. Oceanogr.*, *27*, 581–591.

Blumberg, A. F., and G. L. Mellor (1987), A description of a three-dimensional coastal ocean circulation model, in *Three-Dimensional Coastal Ocean Models*, *Coastal Estuarine Stud.*, vol. 4, edited by N. S. Heaps, pp. 1–16, AGU, Washington, D. C.

Borenäs, K. M., and P. A. Lundberg (1988), On the deep-water flow through the Faroe Bank Channel, *J. Geophys. Res.*, *93*, 1281–1292.

Borenäs, K. M., and P. A. Lundberg (2004), The Faroe-Bank Channel deep water overflow, *Deep Sea Res., Part II*, *51*, 335–350.

Borenäs, K. M., I. L. Lake, and P. A. Lundberg (2001), On the intermediate water masses of the Faroe-Bank Channel overflow, *J. Phys. Oceanogr.*, *31*, 1904–1914.

Bruce, G. J. (1995), Eddies southwest of the Denmark Strait, *Deep Sea Res., Part II*, *42*, 13–29.

Campin, J.-M., and H. Goosse (1999), Parameterization of density-driven downsloping flow for a coarse-resolution ocean model in *z*-coordinate, *Tellus, Ser. A*, *51*, 412–430.

Cenedese, C., J. A. Whitehead, T. A. Ascarelli, and M. Ohiwa (2004), A dense current flowing down a sloping bottom in a rotating fluid, *J. Phys. Oceanogr.*, *34*, 188–203.

Ducet, N., P. Y. Le Tron, and G. Reverdin (2000), Global high-resolution mapping of ocean circulation from TOPEX/Poseidon and ERS-1 and -2, *J. Geophys. Res.*, *105*, 19,477–19,498.

Duncan, L. M., H. L. Bryden, and S. A. Cunningham (2003), Friction and mixing in the Faroe Bank Channel outflow, *Oceanol. Acta*, *26*(5–6), 473–486.

Ezer, T. (2005), Entrainment, diapycnal mixing and transport in three-dimensional bottom gravity current simulations using the Mellor-Yamada turbulence scheme, *Ocean Modell.*, *9*, 151–168.

Ezer, T., and G. L. Mellor (2004), A generalized coordinate ocean model and a comparison of the bottom boundary layer dynamics in terrain-following and in *z*-level grids, *Ocean Modell.*, *6*, 379–403.

Ezer, T., and G. L. Weatherly (1990), A numerical study of the interaction between a deep cold jet and the bottom boundary layer of the ocean, *J. Phys. Oceanogr.*, *20*, 801–816.

Geyer, F., S. Osterhus, D. Quadfasel, and B. Hansen (2005), Faroe Bank Channel outflow: Dynamics of a bottom trapped plume, EGU-2005, *Geophys. Res. Abstr.*, *7*, 07692.

Girton, J. B., and T. B. Sanford (2003), Descent and modification of the overflow plume in the Denmark Strait, *J. Phys. Oceanogr.*, *33*, 1351–1364.

Hallberg, R. W. (2000), Time integration of diapycnal diffusion and Richardson number dependent mixing in isopycnal coordinate ocean models, *Mon. Weather Rev.*, *128*, 1402–1419.

Hansen, B., and S. Østerhus (2000), North Atlantic–Nordic Seas exchanges, *Prog. Oceanogr.*, *45*, 109–208.

Hansen, B., W. Turrel, and S. Østerhus (2001), Decreasing overflow from the Nordic Seas into the Atlantic in the Faroe Bank Channel since 1950, *Nature*, *411*, 927–930.

Hogg, N. G. (1983), Hydraulic control and flow separation in a multi-layered fluid with application to the Vema Channel, *J. Phys. Oceanogr.*, *13*, 695–708.

Høyer, J. L., and D. Quadfasel (2001), Detection of deep overflows with satellite altimetry, *Geophys. Res. Lett.*, *28*(8), 1611–1614.

Jiang, L., and R. W. Garwood Jr. (1996), Three-dimensional simulations of overflows on continental slopes, *J. Phys. Oceanogr.*, *26*, 1214–1233.

Johnson, G. C., and D. R. Ohlsen (1994), Frictionally modified rotating hydraulic channel exchange and ocean outflows, *J. Phys. Oceanogr.*, *24*, 66–78.

Johnson, G. C., and T. B. Sanford (1992), Secondary circulation in the Faroe Bank Channel outflow, *J. Phys. Oceanogr.*, *22*, 927–933.

Jungclaus, J. H., and G. L. Mellor (2000), A three-dimensional model study of the Mediterranean outflow, *J. Mar. Syst.*, *24*, 41–66.

Jungclaus, J. H., J. Hauser, and R. H. Käse (2001), Cyclogenesis in the Denmark Strait overflow plume, *J. Phys. Oceanogr.*, *31*, 3214–3229.

Käse, R. H., J. B. Girton, and T. B. Sanford (2003), Structure and variability of the Denmark Strait Overflow: Model and observations, *J. Geophys. Res.*, *108*(C6), 3181, doi:10.1029/2002JC001548.

Killworth, P. D., and N. R. Edwards (1999), A turbulent bottom boundary layer code for use in numerical models, *J. Phys. Oceanogr.*, *29*, 1221–1238.

Krauss, W. (1996), A note on overflow eddies, *Deep Sea Res., Part I*, *43*, 1661–1667.

Krauss, W., and R. H. Käse (1998), Eddy formation in the Denmark Strait overflow, *J. Geophys. Res.*, *103*, 15,525–15,538.

Lake, I., K. Borenäs, and P. Lundberg (2005), Potential-vorticity characteristics of the Faroe Bank Channel deep-water overflow, *J. Phys. Oceanogr.*, *35*, 921–932.

Legg, S., R. W. Hallberg, and J. B. Girton (2006), Comparison of entrainment in overflows simulated by *z*-coordinate, isopycnal and nonhydrostatic models, *Ocean Modell.*, *11*, 69–97.

Mauritzen, C., J. Price, T. Sanford, and D. Torres (2005), Circulation and mixing in the Faroese Channels, *Deep Sea Res., Part II*, *52*, 883–913.

Mellor, G. L., and T. Yamada (1982), Development of a turbulent closure model for geophysical fluid problems, *Rev. Geophys.*, *20*, 851–875.

Mellor, G. L., S. Hakkinen, T. Ezer, and R. Patchen (2002), A generalization of a sigma coordinate ocean model and an intercomparison of model vertical grids, in *Ocean Forecasting: Conceptual Basis and Applications*, edited by N. Pinardi and J. D. Woods, pp. 55–72, Springer, New York.

Nof, D. (1983), The translation of isolated cold eddies on a sloping bottom, *Deep Sea Res.*, *30*, 171–182.

Nof, D. (1984), Oscillatory drift of cold eddies, *Deep Sea Res.*, *31*, 1395–1414.

Oey, L.-Y. (1998), Eddy energetics in the Faroe-Shetland channel: A model resolution study, *Cont. Shelf Res.*, *17*(15), 1929–1944.

Ozgokmen, T. M., and E. Chassignet (2002), Dynamics of two-dimensional turbulent bottom gravity currents, *J. Phys. Oceanogr.*, *32*, 1460–1478.

Pacanowski, R. C., and A. Gnanadesikan (1998), Transient response in a *z*-level ocean model that resolves topography with partial cells, *Mon. Weather Rev.*, *126*, 3248–3270.

Papadakis, M. P., E. P. Chassignet, and R. W. Hallberg (2002), Numerical simulations of the Mediterranean Sea outflow: Impact of the entrainment parameterization in an isopycnic coordinate ocean model, *Ocean Modell.*, *5*, pp. 325–356, Hooke Inst. Oxford Univ., Oxford, U. K.

Pratt, L. J. (1986), Hydraulic control of sill flow with bottom friction, *J. Phys. Oceanogr.*, *16*, 1970–1980.

Price, J. F., and M. O. Barringer (1994), Outflows and deep water production by marginal seas, *Prog. Oceanogr.*, *33*, 161–200.

Riemenschneider, U., and S. Legg (2005), Regional simulations of the Faroe Bank Channel overflow, EGU-2005, *Geophys. Res. Abstr.*, *7*, 05148.

Saunders, P. M. (1990), Cold outflow from the Faroe Bank Channel, *J. Phys. Oceanogr.*, *20*, 29–43.

Saunders, P. M. (2001), The dense northern overflows, in *Ocean Circulation and Climate: Observing and Modeling the Global Ocean*, edited by G. Siedler, J. Church, and J. Gould, pp. 401–417, Elsevier, New York.

Sherwin, T. J., W. R. Turrel, D. R. G. Jeans, and S. Dye (1999), Eddies and mesoscale deflection of the slope current in the Faroe-Shetland Channel, *Deep Sea Res., Part I*, *46*, 415–438.

Smith, W. H. F., and D. T. Sandwell (1997), Global sea floor topography from satellite altimetry and ship depth soundings, *Science*, *277*, 1956–1962.

Song, Y. T., and Y. Chao (2000), An embedded bottom boundary layer formulation for *z*-coordinate ocean models, *J. Atmos. Oceanic Technol.*, *17*, 546–560.

Spall, M. A., and J. F. Price (1998), Mesoscale variability in Denmark Strait: The PV outflow hypothesis, *J. Phys. Oceanogr.*, *28*, 1598–1623.

Swaters, G. E. (2003), Baroclinic characteristics of frictionally destabilized abyssal overflows, *J. Fluid Mech.*, *489*, 349–379.

Winton, M., E. W. Hallberg, and A. Gnanadesikan (1998), Simulation of density-driven frictional downslope flow in *z*-coordinate ocean models, *J. Phys. Oceanogr.*, *28*, 2163–2174.

T. Ezer, Program in Atmospheric and Oceanic Sciences, P.O. Box CN710, Sayre Hall, Princeton University, Princeton, NJ 08544-0710, USA. (ezer@splash.princeton.edu)